ARTICLE

Aerosol synthesis of phase pure iodine/iodic biocide microparticles

Tao Wu, Andrew SyBing, Xizheng Wang, and Michael R. Zachariah[a)]
Department of Chemistry and Biochemistry and Department of Chemical and Biomolecular Engineering, University of Maryland, College Park, MD 20742, USA

(Received 6 October 2016; accepted 28 December 2016)

High iodine containing oxides are of interest as biocidal components in energetic applications requiring fast exothermic reactions with metallic fuels. Aerosol techniques offer a convenient route and potentially direct route for preparation of small particles with high purity, and are a method proven to be amenable and economical to scale-up. Here, we demonstrate the synthesis of various iodine oxide/iodic acid microparticles by a direct one-step aerosol method from iodic acid. By varying temperature and humidity, we produced near phase pure δ-HIO_3, HI_3O_8, and I_2O_5 as determined by X-ray diffraction. δ-HIO_3, a previously unknown phase, was confirmed in this work. In addition, scanning electron microscopy was used to examine the morphology and size of those prepared iodine oxide/iodic acid particles and the results show that all particles have an irregularly spherical shape. Thermogravimetric/differential scanning calorimetry measurement results show that HIO_3 dehydrates endothermically to HI_3O_8, and then to I_2O. I_2O_5 decomposes to I_2 and O_2.

I. INTRODUCTION

In recent years, the interest in developing new energetic materials with biocidal capabilities[1,2] has drawn increased attention.[3–13] The motivation for this is based on evidence that conventional energetic materials, which employ a thermal neutralization mechanism, are not sufficiently efficient.[14] Laboratory studies have demonstrated that the addition of a biocidal component can significantly enhance neutralization through a synergistic mechanism.[15–20] Therefore, it has been proposed that simultaneously delivering a rapid thermal pulse with a remnant biocidal agent would prolong the exposure time and improve the inactivation process.[21] Both halogens and silver-containing energetic materials have been explored[22–24] with the halogens offering the most promise due to their excellent biocidal properties.[25] Various methods have been used for incorporating halogens into energetic materials. One approach is through directly introducing halogens into the system and the other is by incorporating halogens into the oxidizers.[25,26] Thus, iodine-rich compounds that can release HI or I_2 are the ideal candidates for biocidal energetics.[27]

Iodine (V) oxide, as one of the iodine-containing oxides with ~76% iodine mass fraction, has been recently studied as an oxidizer with aluminum fuel.[28] In this case, various metals (primarily aluminum) are mixed with I_2O_5 to form a thermite system whose combustion properties were studied.[29–32] The first paper concerning the reactivity between aluminum and I_2O_5 was published by Ivanov et al. in 1980 in which a global reaction mechanism between iodine gas and fuels was proposed[29] and confirmed in a later work.[32] I_2O_5 has received considerable interest because it is an extremely aggressive oxidizer with aluminum with reported propagation velocities up to ~2000 m/s for loose ball-milled nano-aluminum and nano-scaled I_2O_5 (~10 nm).[31] In addition, constant volume combustion tests on nano-Al/micro-I_2O_5 thermite exhibit the highest pressurization rate and the shortest burn time relative to other aluminum based traditional thermites such as Al/CuO and Al/Fe_2O_3.[32]

Moreover, oxoacids of iodine, such as HIO_3 and HI_3O_8, have been investigated in the recent decades. Until now, two polymorphs of iodic acid, the stable α-HIO_3[33,34] and metastable γ-HIO_3,[35] have been reported and well-characterized. However, more evidence is required to verify the existence of β-HIO_3.[35] The thermal behavior of HIO_3 was studied via thermogravimetric analysis/differential scanning calorimetry (TGA/DSC) and the result shows three decomposition steps upon heating in air: the dehydration of HIO_3 into HI_3O_8 at 100 °C, the dehydration of HI_3O_8 into I_2O_5 at 210 °C, and the melting/decomposition of I_2O_5 at 400 °C.[36] It also reveals that I_2O_5 would be slowly converted to the initial hydrate HI_3O_8 and later to the final hydrate HIO_3 under ambient environment. Furthermore, the crystal structure of HI_3O_8 was determined to be an adduct $HIO_3 \cdot I_2O_5$, which are connected by hydrogen bonds.[37]

Aerosol techniques offer a convenient route and potentially direct route for the preparation of nano-sized or micro-sized particles with high purity, and are a method

Contributing Editor: Gary L. Messing
[a)]Address all correspondence to this author.
e-mail: mrz@umd.edu
DOI: 10.1557/jmr.2017.6

proven to be amenable and economical to scale-up. Along with the fact that decreasing the size of oxidizer particles can improve the burn rate of thermite,[32] in this study we develop a synthesis approach to prepare various iodine oxide/iodic acid microparticles based on aerosol spray pyrolysis (ASP) using commercial iodic acid (HIO_3) as the starting material, because of its water solubility and ready availability.[38] The decomposition behavior of iodine oxides/iodic acids was also studied using low heating rates with TGA/DSC.

II. EXPERIMENTAL

A. Materials

Iodic acid (HIO_3) (99.5 wt%) purchased from Sigma-Aldrich (St. Louis, Missouri) was directly used as received. All the other chemicals were of analytical grade and used as purchased without further treatment.

B. Preparation of various iodine oxide/iodic acid particles via aerosol spray pyrolysis

Small-sized particles of oxides were obtained via ASP. In general, 100 mL iodic acid aqueous solution (10 mg/mL) was sprayed into small droplets (~1 μm in diameter) with a home-made pressure atomizer (~35 pounds per square inch (psi) pressure air) and passed through a silica-gel diffusion drier (silica gels were regenerated at ~50 °C or 80 °C to prepare different products) to remove water and are then passed through a tube furnace for chemical conversion. The tube reactor consisted of an ~1.9 cm diameter alumina tube with a heated length of ~40 cm. The furnace temperature was set at ~230 and ~375 °C to obtain either δ-HIO_3 or I_2O_5, respectively, with a residence time of about 1 s.[39] For both δ-HIO_3 and I_2O_5, silica gels were regenerated at 50 °C. We find that δ-HIO_3 can be obtained within a large range of temperature from 210 to 250 °C. In addition, HI_3O_8 was obtained with a tube furnace temperature ~250 °C and silica gels regeneration temperature ~80 °C. The final product was collected on a Millipore membrane filter (0.4 μm pore) and characterized by scanning electron microscopy (SEM; SU-70 FEG-SEM, Hitachi Corp., Tokyo, Japan) and powder X-ray diffraction (XRD; Bruker D8 Advance, Bruker Corporation, Billlerica, Massachusetts, using Cu K_α radiation).

C. *In situ* heating XRD measurement

In situ heating XRD was performed using a Bruker C2 diffractometer with a Vantec500 2D detector with 2θ ranging from 10° to 50° (λ = 1.5418 Å, step size = 0.05°) and the sample was heated via an Anton Paar DHS 1100 graphite-dome hot stage with a heating rate of 10 °C/min under air condition. We collected patterns at 26, 100, 200, 300, 400, and 500 °C and also collected a final pattern at 30 °C after the sample was cooled. At each temperature, we collected two 10 min frames at 20 and 40° 2θ. Integrating and merging the two frames together gave us a final powder diffraction pattern from 9.5° to 50° 2θ.

D. TGA/DSC measurement

TGA and DSC were conducted using a SDT Q600 (TA Instruments, New Castle, Delaware) equipped with a TA Discovery MKS104-S0212004 Micro Vision 2 mass spectrometer (TA Instruments). The analysis was performed under a 100 mL/min argon flow with ~1.0 mg samples placed into an alumina pan and heated from room temperature up to 550 °C at a rate of 5 °C/min in argon atmosphere.

III. RESULT AND DISCUSSION

Iodic acid (HIO_3) is a white solid at room temperature and is often used as the starting material for preparing iodine-containing materials due to its ready availability, high solubility in water, and that with controlled dehydration yields iodine oxides.

Atomized aqueous HIO_3 droplets in air were passed through a silica gel diffusion dryer to produce solid HIO_3 particles which were then directly passed through the tube furnace at a desired temperature to form various iodine oxide/iodic acids (Fig. 1). To determine what temperature should be run for the regeneration of silica gels, thermal analysis was conducted on a fully hydrated silica gel and the result is shown in Fig. 2. The black line represents the mass change of the silica gel with

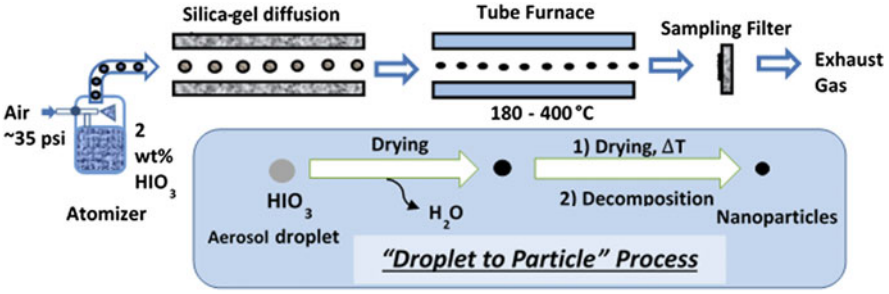

FIG. 1. Aerosol spray pyrolysis to synthesize various iodine oxides/iodic acids.

increasing temperature. From this, we note that the silica gel reaches its fully dehydrated state after 15% weight loss (water loss). Assuming a fully dehydrated silica gel has a weight of 85 mg, it could absorb 15 mg of water to reach its fully hydrated state (100 mg weight).

For silica $gel_{m=85\ mg}$ regenerated at 50 and 80 °C, they could absorb 4.4 and 8 mg of water, respectively, to reach their fully hydrated state based on the TGA result in Fig. 2. Since silica gels obtained from different regeneration temperatures have different water-absorbing capabilities, silica-gels regeneration temperature also plays an important role in the aerosol route. In this work, regeneration temperatures of ~50 and 80 °C were used to obtain different products to change the water absorbing properties.

Since iodic acid droplets pass through the tube furnace where the thermal event occurs, we use TGA/DSC results to determine set points for the furnace. Figure 3 shows

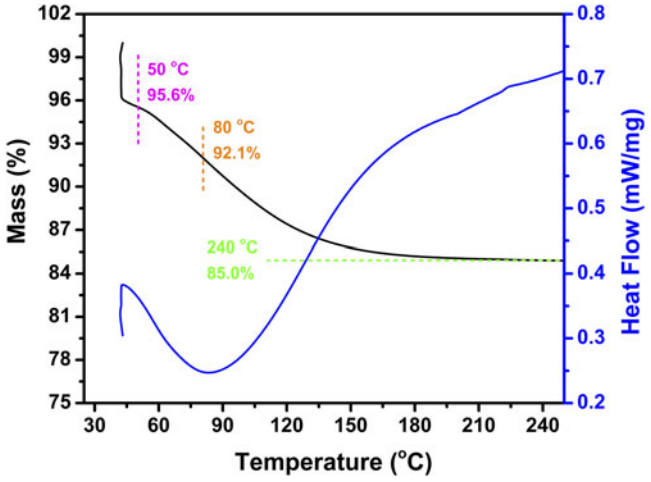

FIG. 2. The TGA and DSC curves of a fully hydrated silica gel under argon environment at a heating rate of 5 °C/min.

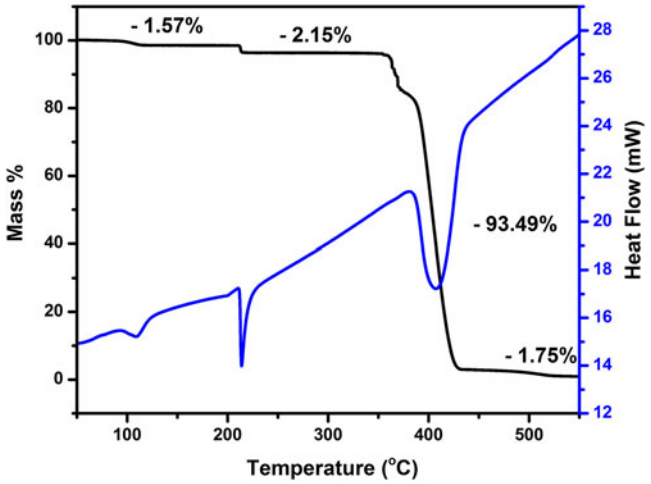

FIG. 3. TGA and DSC curves of HIO_3 under air environment at a heating rate of 5 °C/min.

the TGA and DSC curves of iodic acid under air environment with a heating rate of 5 °C/min, which indicates that there are three decomposition steps: the dehydration of HIO_3 to HI_3O_8 at ~120 °C, dehydration of HI_3O_8 to I_2O_5 at ~210 °C, and the decomposition of I_2O_5 at 380 °C. Thus, I_2O_5 and HI_3O_8 could be obtained via thermal treatment at 210–380 °C and 120–210 °C, respectively. The thermal behavior of HIO_3 under argon was very similar to the air case and the detailed information is shown in Fig. S2.

The residence time for a droplet in the aerosol reactor is about 1 s, which is obviously much shorter than that in the TGA ramp time. To obviate this effect we ran the furnace temperature higher than what the TGA would indicate to speed up the kinetics. To validate the phases indicted in the TGA, *in situ* hot-stage XRD was performed on the HIO_3 powder at a heating rate of 10 °C/min from room temperature to 500 °C in air. From Table I, I_2O_5 and HI_3O_8 could be obtained at 300–400 °C and 200–300 °C, respectively. The XRD patterns of HIO_3 at different temperatures are provided in Fig. S3.

A. Preparation of I_2O_5

I_2O_5 [Fig. 4(c)] was obtained when the tube furnace was set at 350–400 °C which is consistent with the TGA result in Fig. S1. TGA and DSC curves of I_2O_5 [Fig. 4(d)] show the characteristically endothermic decomposition of I_2O_5 into I_2 and O_2 at ~360 °C which also proves the formation of I_2O_5. The small weight loss at ~210 °C indicates that small amount of I_2O_5 product is probably rehydrated into HI_3O_8 during the collection process and preparation for TGA/DSC test. The SEM images [Figs. 4(a) and 4(b)] show that I_2O_5 particles are irregularly spherical and some large aggregates are also observed in those images indicating that some sintering/coalescence between particles takes place.

B. Preparation of δ-HIO_3

Based on the thermal behavior of HIO_3, HI_3O_8 could be obtained when the tube furnace was set at 120–210 °C. Considering the short residence time within the whole aerosol process and the difference between theoretical and experimental temperatures for preparing I_2O_5, the furnace temperature for the synthesis of HI_3O_8 was set higher at 210–250 °C.

The XRD [Fig. 5(a)] spectra of the as-prepared iodine oxide were consistent with an XRD pattern previously identified as $I_4O_9{\cdot}xH_2O$ (PDF#45-0872), with no

TABLE I. The chemical composition of HIO_3 during *in situ* heating XRD test at different temperatures in air.

Temperature (°C)	26	100	200	300	400	500
Product(s)	HIO_3	HIO_3, HI_3O_8	HI_3O_8	I_2O_5	I_2O_5	$I_2 + O_2$

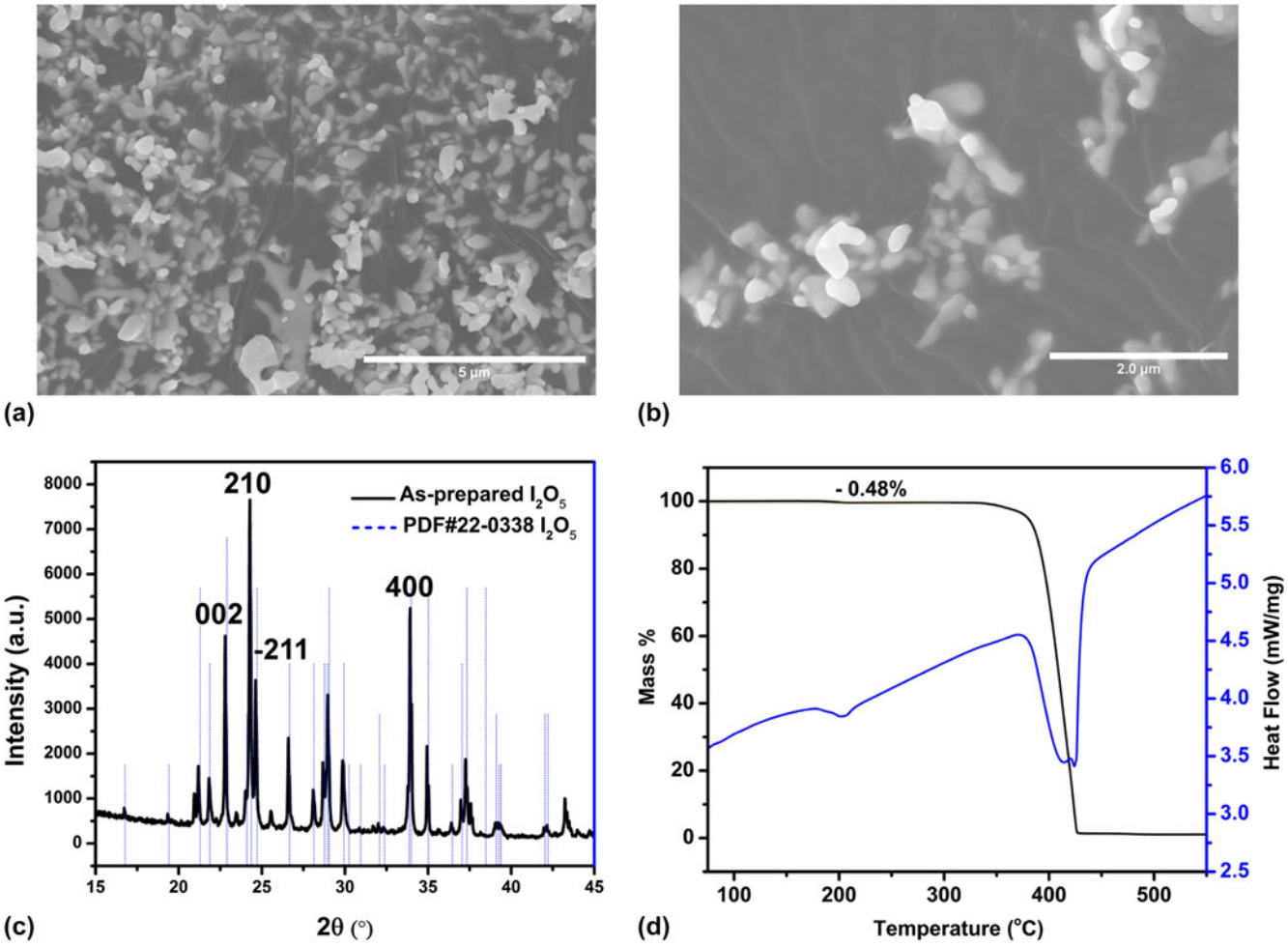

FIG. 4. SEM image (a and b), XRD pattern (c), TGA and DSC (Ar, 5 °C/min) (d) of as-prepared I_2O_5.

indication of any other iodine oxide/iodic acid. Like I_2O_5 particles, the SEM images [Figs. 5(b) and 5(c)] show that "$I_4O_9{\cdot}xH_2O$" particles are irregularly spherical due to the sintering/coalescence between particles. This is also confirmed because the resulting particles are larger than expected based on the initial droplet size and concentration used and were nominally ~400 nm in diameter.

The proposed structure implies that xH_2O could be removed via vacuum drying. However, TGA/DSC and XRD results shown in Fig. S4 indicated surprisingly that there were no changes after vacuum drying. Moreover, the TGA and DSC results of $I_4O_9{\cdot}xH_2O$ shown in Fig. S4 are very similar to those of HIO_3 (Fig. S2), and this similar behavior was further confirmed with *in situ* heating XRD (Table II). Given that the previous report proposed the formula $I_4O_9{\cdot}xH_2O$ without any chemical composition or any crystal structure information,[40] we conjecture that the proposed formula may be in error.

Based on its powder XRD pattern, we find a distorted octahedral crystal system, space group $P_{2_12_12_1}$ which consists of IO_3 ions with three I–O bonds with distances of 1.78, 1.80, and 1.92 Å, and three I–O contacts with distances of 2.51, 2.76, and 2.76 Å. This reveals that the correct assignment of the phase is actually a previously unreported phase of HIO_3, which we refer to as δ-HIO_3. The detailed crystal information will be published separately. In addition, the difference between XRD patterns (Fig. S4) of as-prepared δ-HIO_3 and as-received HIO_3 also suggests a new phase HIO_3.

Thus, instead of obtaining HI_3O_8, as the TGA results would suggest we obtain δ-HIO_3 which indicates that the decomposition pathways of HIO_3 in TGA (slow heating) and ASP (fast heating) are different. This result implies that the δ-HIO_3 is metastable at elevated temperatures and at slow heating converts to I_2O_5. The ASP process enables a rapid thermal ramp and rapid quench to trap the material as δ-HIO_3 which appears to be quite stable at room temperature. In fact, I_2O_5 was obtained when the furnace temperature was raised to above 300 °C.

C. Preparation of HI_3O_8

Based on the result in Fig. 3, we are expecting to obtain HI_3O_8 by thermal treatment of HIO_3 at temperatures

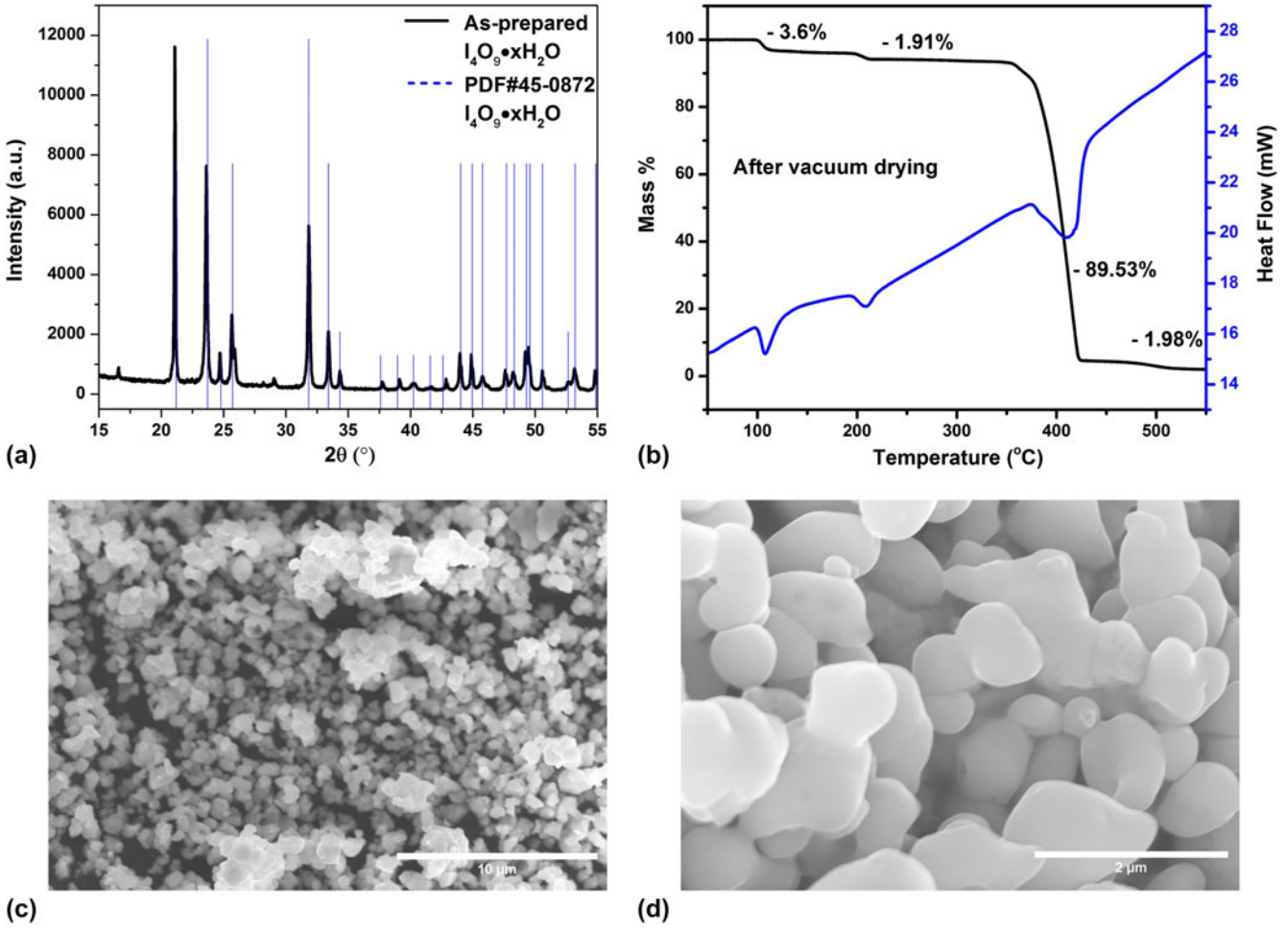

FIG. 5. XRD pattern (a), TGA/DSC (b), and SEM images (c and d) of as-prepared $I_4O_9 \cdot xH_2O$ after vacuum drying treatment.

TABLE II. The chemical composition of "$I_4O_9 \cdot xH_2O$" during *in situ* heating XRD test at different temperatures in argon environment.

Temperature (°C)	26	100	200	300–400	500
Product(s)	"$I_4O_9 \cdot xH_2O$"	"$I_4O_9 \cdot xH_2O$", HI_3O_8	HI_3O_8	I_2O_5	$I_2 + O_2$

between 120 and 210 °C in air. Therefore, we annealed HIO_3 at different temperatures in air for one hour and it turns out that HIO_3 was fully dehydrated to HI_3O_8 at 150–260 °C (Fig. S5). Surprisingly, HI_3O_8 was obtained after only two minutes annealing at ~165 °C (Fig. S5), which indicates that the dehydration of HIO_3 is fast and also suggests that ASP is a promising method to prepare HI_3O_8.

Previous results show that δ-HIO_3 rather than HI_3O_8 is the product when the tube furnace was set between 210 and 250 °C with silica gels regenerated at ~50 °C. Considering HI_3O_8 is a dehydrated product of HIO_3, the failure to prepare HI_3O_8 might be caused by the relatively weak dehydrating capacity of the original setup. Again, I_2O_5 appeared when the tube furnace was increased to 300 °C or above. This suggested that tuning the tube furnace temperature alone could not obtain HI_3O_8. From the previous discussion, we know that the silica gel regeneration temperature also affects the aerosol synthesis and might be used to manipulate the hydrating ability of the setup. We found that regenerating the silica gel at ~80 °C rather than ~50 °C would form HI_3O_8 as confirmed by XRD [Fig. 6(a)] in a single step with a tube furnace temperature of ~250 °C. The TGA shown in Fig. 6(b) indicates two decomposition steps: one is the dehydration of HI_3O_8 to I_2O_5 at ~210 °C with an experimental weight loss of 1.2% (theoretical weight loss, 1.8%; impurities, ~6%); another is the decomposition of I_2O_5 at ~360 °C, both of which are endothermic as determined by DSC. Similar to δ-HIO_3, the SEM images of HI_3O_8 in Figs. 6(c) and 6(d) show that particles are irregular spheres due to sintering/coalescence between particles during preparation.

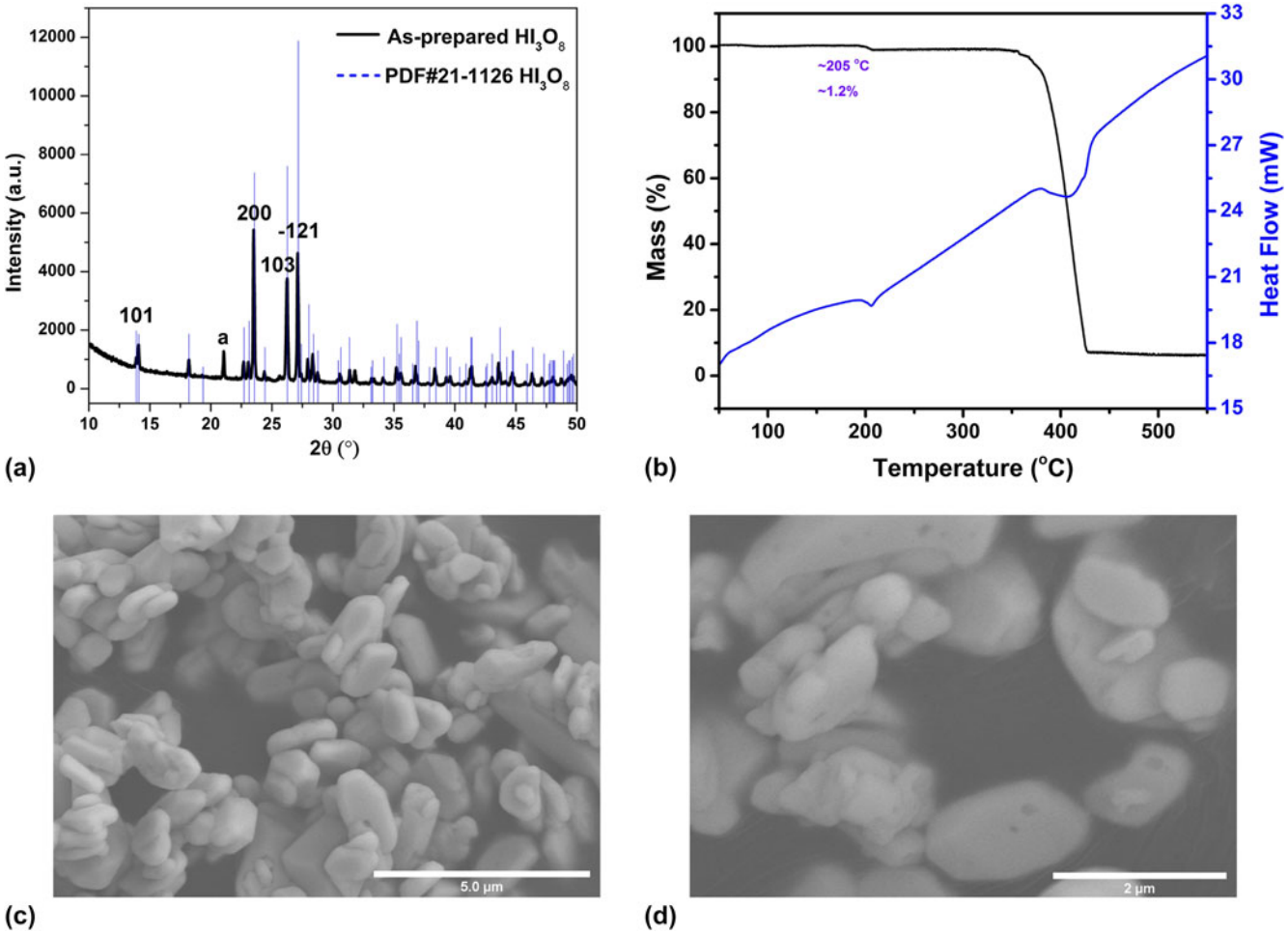

FIG. 6. XRD pattern (a), TGA/DSC[a] (b), and SEM images (c and d) of as-prepared HI_3O_8. ([a]: Ran under argon environment at a heating rate of 5 °C/min.)

TABLE III. Summarizing the parameters of ASP for preparing different products.

Parameters | products	I_2O_5	δ-HIO_3	HI_3O_8
Silica gel regeneration temperature (°C)	50	50	80
Furnace temperature (°C)	350–400	210–250	~250

IV. CONCLUSIONS

In summary three different products, δ-HIO_3, HI_3O_8, and I_2O_5, were obtained via ASP as summarized in Table III. Both temperature and humidity control in silica gel preparation were necessary to obtain all three products without post-processing. For temperatures not listed in Table III, either mixtures (HIO_3/HI_3O_8/I_2O_5) or no product was collected.

This study demonstrates a facile and environment-friendly aerosol spray pyrolysis method to prepare various iodine oxides/iodic acids using a single precursor HIO_3. By tuning the furnace temperature and the humidity, we were able to produce near phase pure δ-HIO_3, HI_3O_8, and I_2O_5 as determined by XRD in a single step. TGA and DSC results show that HIO_3 dehydrates to HI_3O_8, and then I_2O_5, and lastly I_2O_5 decomposes endothermically into I_2 and O_2.

REFERENCES

1. R-D. Chapman, D. Thompson, G. Ooi, D. Wooldridge, P-N. Cash, and R-A. Hollins: Presented at the *Joint 66th Southwest and 62nd Southeast Regional Meeting of the American Chemical Society*, New Orleans, LA, December, 2012.
2. K-T. Sullivan, C-W. Wu, N-W. Piekiel, K. Gaskell, and M-R. Zachariah: Synthesis and reactivity of nano-Ag_2O as an oxidizer for energetic systems yielding antimicrobial products. *Combust. Flame* **160**(2), 438 (2013).
3. M. Schoenitz, T-S. Ward, and E-L. Dreizin: Fully dense nano-composite energetic powders prepared by arrested reactive milling. *Proc. Combust. Inst.* **30**, 2071 (2005).
4. K-J. Blobaum, A-J. Wagner, J-M. Plitzko, D. Van Heerden, D-H. Fairbrother, and T-P. Weihs: Investigating the reaction path and growth kinetics in CuO_x/Al multilayer foils. *J. Appl. Phys.* **94**, 2923 (2003).
5. K. Zhang, C. Rossi, and G-A. Ardila Rodriguez: Development of a nano-Al/CuO based energetic material on silicon substrate. *Appl. Phys. Lett.* **91**, 113117 (2007).

6. S-M. Umbrajkar, S. Seshadri, M. Schoenitz, V-K. Hoffmann, and E-L. Dreizin: Aluminum-rich Al–MoO_3 nanocomposite powders prepared by arrested reactive milling. *J. Propul. Power* **24**, 192–198 (2008).
7. T-S. Ward, W. Chen, M. Schoenitz, R-N. Dave, and E-L. Dreizin: A study of mechanical alloying processes using reactive milling and discrete element modeling. *Acta Mater.* **53**, 2909–2918 (2005).
8. S-H. Kim and M-R. Zachariah: Enhancing the rate of energy release from nanoenergetic materials by electrostatically enhanced assembly. *Adv. Mater.* **16**, 1821 (2004).
9. T-M. Tillotson, A-E. Gash, R-L. Simpson, L-W. Hrubesh, J-H. Satcher, Jr., and J-F. Poco: Nanostructured energetic materials using sol−gel methodologies. *J. Non-Cryst. Solids* **285**, 338 (2001).
10. H-S. Seo, J-K. Kim, J-W. Kim, H-S. Kim, and K-K. Koo: Thermal behavior of Al/MoO_3 xerogel nanocomposites. *J. Ind. Eng. Chem.* **20**, 189 (2014).
11. C. Rossi, K. Zhang, D. Esteve, P. Alphonse, P. Tailhades, and C. Vahlas: Nanoenergetic materials for MEMS: A review. *J. Microelectromech. Syst.* **16**, 919 (2007).
12. J-Y. Malchi, T-J. Foley, and R-A. Yetter: Electrostatically self-assembled nanocomposite reactive microspheres. *ACS Appl. Mater. Interfaces* **1**, 2420 (2009).
13. H-Y. Wang, G-Q. Jian, G-C. Egan, and M-R. Zachariah: Assembly and reactive properties of Al/CuO based nanothermite microparticles. *Combust. Flame* **161**, 2203 (2014).
14. K. Sullivan, N. Pickiel, S. Chowdhury, C. Wu, C. Johnson, and M.R. Zachariah: Ignition and combustion characteristics of nanoscale Al/$AgIO_3$: A potential energetic biocidal system. *Combust. Sci. Technol.* **183**, 205 (2011).
15. W. Zhou, M-W. Orr, V-T. Lee, and M-R. Zachariah: Synergistic effects of ultrafast heating and gaseous chlorine on the neutralization of bacterial spores. *Chem. Eng. Sci.* **144**, 39 (2016).
16. W. Zhou, M-W. Orr, G. Jian, S. Watt, V-T. Lee, and M-R. Zachariah: Inactivation of bacterial spores subjected to sub-second thermal stress. *Chem. Eng. J.* **279**, 578 (2015).
17. F-T. Tabit and E. Buys: The effects of wet heat treatment on the structural and chemical components of Bacillus sporothermodurans spores. *Int. J. Food Microbiol.* **140**, 207 (2010).
18. S. Zhang, M. Schoenitz, and E-L. Dreizin: Mechanically alloyed Al–I composite materials. *J. Phys. Chem. Solids* **71**, 1213 (2010).
19. S. Zhang, M. Schoenitz, and E-L. Dreizin: Iodine release, oxidation, and ignition of mechanically alloyed Al−I composites. *J. Phys. Chem. C* **114**, 19653 (2010).
20. S. Zhang, C. Badiola, M. Schoenitz, and E-L. Dreizin: Oxidation, ignition, and combustion of Al·I_2 composite powders. *Combust. Flame* **159**, 1980 (2012).
21. H. Wang, G. Jian, W. Zhou, J. DeLisio, V. Lee, and M-R. Zachariah: Metal iodate-based energetic composites and their combustion and biocidal performance. *ACS Appl. Mater. Interfaces* **7**, 17363 (2015).
22. C-E. Johnson and K-T. Higa: *Iodine Rich Biocidal Reactive Materials*. Presented at MRS Meeting, Boston, **11**, 25 (2012).
23. O. Mulamba, E-M. Hunt, and M-L. Pantoya: Neutralizing bacterial spores using halogenated energetic reactions. *Biotechnol. Bioprocess Eng.* **18**, 918 (2013).
24. C. He, J. Zhang, and J-M. Shreeve: Dense iodine-rich compounds with low detonation pressures as biocidal agents. *Chem. –Eur. J.* **19**, 7503 (2013).
25. Y. Aly, S. Zhang, M. Schoenitz, V-K. Hoffmann, E-L. Dreizin, M. Yermakov, R. Indugula, and S-A. Grinshpun: Iodine-containing aluminum-based fuels for inactivation of bioaerosols. *Combust. Flame* **161**, 303 (2014).
26. J-Y. Feng, G-Q. Jian, Q. Liu, and M-R. Zachariah: Passivated iodine pentoxide oxidizer for potential biocidal nanoenergetic applications. *ACS Appl. Mater. Interfaces* **5**, 8875 (2013).
27. D. Fischer, T-M. Klapçtke, and J. Stierstorfer: Synthesis and characterization of guanidinium difluoroiodate, $[C(NH_2)_3]^+[IF_2O_2]^-$ and its evaluation as an ingredient in agent defeat weapons. *Anorg. Allg. Chem.* **637**, 660 (2011).
28. K-S. Martirosyan: Nanoenergetic gas-generators: Principles and applications. *J. Mater. Chem.* **21**, 9400 (2011).
29. B-K. Little, E-J. Welle, S-B. Emery, M-B. Bogle, V-L. Ashley, A-M. Schrand, and M-C. Lindsay: Chemical dynamics of nano-aluminum/iodine (V) oxide. *J. Phys. Conf. Ser.* **500**(5), 052025 (2014).
30. C. Farley and M. Pantoya: Reaction kinetics of nanometric aluminum and iodine pentoxide. *J. Therm. Anal. Calorim.* **102**, 609 (2010).
31. K-S. Martirosyan, L. Wang, and D. Luss: Development of nanoenergetic materials based on Al/I_2O_5 system. In *Nanotech 2010*, Vol. 2 (NSTI, Austin, 2010); pp. 137–140.
32. G. Jian, S. Chowdhury, J. Feng, and M-R. Zachariah: The ignition and combustion study of NanoAl and iodine pentoxide thermite. In *Joint Meeting - US Sections of the Combustion Institute*, Vol. 2 (Curran Associaties Inc., Red Hook, 2013); pp. 1287–1299.
33. K. Stahl and M-A. Szafranski: Single-crystal neutron diffraction study of HIO_3 at 295 and 30 K and of DIO_3 at 295 K. *Acta Chem. Scand.* **46**, 1146 (1992).
34. M-T. Rogers and L. Helmholz: The crystal structure of iodic acid. *J. Am. Chem. Soc.* **63**, 278 (1941).
35. A. Fischer and M. Lindsjö: γ-HIO_3—A metastable, centrosymmetric polymorph of iodic acid. *Z. Anorg. Allg. Chem.* **631**, 1574 (2005).
36. B-K. Little, S-B. Emery, J-C. Nittinger, R-C. Fantasia, and M-C. Lindsay: Physiochemical characterization of iodine (V) oxide, Part 1: Hydration rates. *Propellants. Explos. Pyrotech.* **40**, 595 (2015).
37. A. Fischer: Redetermination of HI_3O_8, an adduct of formula $HIO_3·I_2O_5$. *Acta Cryst.* **E61**, i278 (2005).
38. C-M. Sorensen, Q. Li, H-K. Xu, Z-X. Tang, K-J. Klabunde, and G-C. Hadjipanayis: Aerosol spray pyrolysis synthesis techniques. *Nanophase Materials* **260**, 109 (1994).
39. L. Liu, M-R. Zachariah, S-I. Stoliarov, and J. Li: Enhanced thermal decomposition kinetics of poly(lactic acid) sacrificial polymer catalyzed by metal oxide nanoparticles. *RSC Adv.* **5**, 101745 (2015).
40. A. Wikjord, P. Taylor, D. Torgerson, and L. Hachkowski: Thermal behavior of corona-precipitated iodine oxides. *Thermochim. Acta* **36**, 367 (1980).

Supplementary Material

To view supplementary material for this article, please visit https://doi.org/10.1557/jmr.2017.6.